Spectroscopy and Structure of Bacteriochlorophyll Dimers. I. Structural Consequences of Nonconservative Circular Dichroism Spectra

M. H. C. Koolhaas,* G. van der Zwan,* F. van Mourik,# and R. van Grondelle#
*Department of Theoretical and Physical Chemistry and #Department of Physics and Astronomy, Vrije Universiteit, 1081 HV Amsterdam, The Netherlands

ABSTRACT The origin of the nonconservative nature of the circular dichroism (CD) spectrum of bacteriochlorophyll dimers is investigated. It is shown that coupling between the Q_y and Q_x transitions can, under rather restricting circumstances, lead to an asymmetrical CD spectrum: only for a limited set of relative orientations of the monomers within the dimer is the spectrum found to be asymmetrical. The relation between intensity and asymmetry of the CD spectrum is elucidated. The results are applied to the B820 subunit of the LH1 antenna system and subsequently to the antenna system LH1 itself. Differences in the geometry of the BChls in LH1 versus the LH2 structure are discussed.

INTRODUCTION

The bacteriochlorophyll (BChl) dimer is ubiquitous in the photosynthetic apparatus of photosynthetic bacteria. In the reaction center of photosynthetic purple bacteria, the special pair of BChl molecules acts as the primary electron donor P, which upon excitation drives an ultrafast charge separation process. In both the core LH1 and the peripheral light-harvesting antenna, LH2, the basic building block is the $\alpha\beta$ subunit, which in its transmembrane hydrophobic part binds a dimer of BChl molecules. Recently the structure of the LH2 complex of *Rhodopseudomonas acidophila* has been determined by McDermott et al. (1995) by means of X-ray spectroscopy with a resolution of ~2.5 Å. The complex exhibits a ninefold symmetry, and in this structure the nine α and nine β polypeptides are arranged in two concentric rings with the 18 B850 BChls sandwiched between them, and their Q_y dipoles parallel and their Q_x dipoles perpendicular to the plane of the ring. Close to the periplasmic side of the complex a ring of nine "monomeric" BChls is arranged with their macrocycles more or less parallel to the membrane plane. Two B850 BChls are at a typical center-to-center distance of about 1 nm, two B800 BChls at about 2.1 nm, and the two rings are about 1.8 nm apart.

Similar features are observed for the core light-harvesting complex LH1. An 8.5-Å structure of *Rhodospirillum rubrum* obtained by Karrasch et al. (1995) exhibits a 16-fold symmetry axis with the 16 α and 16 β polypeptides arranged in a manner very similar to that of LH2. However, the resolution of the LH1 structure is not high enough to establish the arrangement of the 32 BChls within the LH1 ring. However, from linear dichroism and polarized fluorescence measurements it follows that the global organization (Kramer et al., 1984b) of the BChls in LH1 must be similar to that in LH2. The conservative character of the CD spectrum of LH2 and the nonconservative features of the CD of LH1 suggest differences in the two ring structures, as will be shown in this article. The number of $\alpha\beta$ units that form a LH1 ring may be variable (Kühlbrandt, 1995). From LH1 a subunit can be purified that consists of only the $\alpha\beta$ heterodimer and two BChls. The subunit absorbs at 820 nm and has all the properties of an excitonically coupled dimer. The upper and lower exciton components can be identified in the CD and polarized fluorescence excitation spectra and triplet minus singlet measurements (Visschers et al., 1991; Van Mourik et al., 1991), and the excitonic coupling between the pair of BChls is about 230 cm^{-1}. From a variety of experiments it became evident that the absorption bandwidth was largely dominated by inhomogeneous broadening (Visschers et al., 1992, 1993; De Caro et al., 1994; Pullerits et al., 1995), and a variety of spectral properties of B820 were explained in terms of the "disordered dimer" model (Van Mourik et al., 1992; Koolhaas et al., 1994). Whether the dimer properties survive upon ring formation is a matter of experimental and theoretical debate. Of course, the progressive redshift upon ring formation suggests increased excitonic interaction. On the other hand, it is well established, for instance, that variations in the H-bonding pattern of the BChl dimer in LH2 introduced by mutations can shift the absorption from 850 nm back to 820 nm (Fowler et al., 1992, 1994), most likely without affecting the properties of the ring.

Recently the energy transfer dynamics in LH1 and LH2 were monitored on a subpicosecond time scale by observing the dynamic redshift of the transient absorption of the spectrum (Visser et al., 1995) and the time-resolved fluorescence depolarization (Bradforth et al., 1995; Jimenez et al., 1996). Both phenomena could be very well explained on the basis of a model that assumes hopping of the excitation in a ring of inhomogeneously broadened dimers. The single-site lifetime was estimated to be slightly below 100 fs for LH1 (Visser et al., 1995; Bradforth et al., 1995) and even shorter for LH2 (Jimenez et al., 1996). The red shift of the

Received for publication 20 May 1996 and in final form 30 December 1996.

Address reprint requests to Dr. M. H. C. Koolhaas, Department of Theoretical and Physical Chemistry, Vrije Universiteit, De Boelelaan 1083, 1081 HV Amsterdam, The Netherlands. Tel.: 31-204447644; Fax: 31-204447643; E-mail: koolhaas@chem.vu.nl.

0006-3495/97/04/1828/14 $2.00

zero crossing of the CD spectrum of LH2 versus its absorption maximum, however, suggests a larger spectroscopic unit than two BChls (Sauer et al., 1996; Somsen et al., 1996). Therefore it is important to establish both the precise number of B820 subunits in LH1/LH2 and the geometrical orientation of the BChl molecules within a single unit for understanding the relevant spectral features, and the way in which the excitations are transported and finally delivered to the special pair.

In this paper we extend the work of Scherz and Parson (1984, 1986), who performed similar calculations but concentrated on systems with almost symmetrical CD spectra. So, although they did in fact mention the possibility of an asymmetrical CD as a consequence of the Q_y-Q_x coupling, this was not used as a method to obtain structural information for the dimer. The BChl dimers are usually referred to as excitonically coupled dimers, because the spectroscopic properties can be derived by using an interaction Hamiltonian that couples the monomers through their transition dipole moments (Craig and Thirunamachandran, 1984). The simplest possible model, considering the dimer as a combination of two-level systems, can explain a number of spectroscopic features of such systems. The exciton coupling leads to lines, with small separation, in the absorption spectrum, and the distance between the lines is a direct measure of the coupling matrix elements (Broude et al., 1985). The same model can also be used to calculate the CD spectrum, but there it fails to explain one prominent feature, namely that most CD spectra are asymmetrical or, in other words, nonconservative (Scherz et al., 1990). Asymmetry can result from magnetic contributions of the monomers to the spectrum (Cantor and Schimmel, 1980), but the intensity of the CD spectrum of monomeric BChl is very small (Parkes-Loach et al., 1988), so the magnetic contribution is invariably very small to absent, and one has to search for another explanation.

In this paper we attribute the asymmetry of the CD spectrum to the exciton coupling between different levels of the monomers. The monomers are considered to be N-level systems, and we will show how various coupling matrix elements can be used to explain the asymmetry and intensity of the CD spectrum, and how the relative intensities of the various transitions are modified by changing the coupling matrix elements. The magnitude of the various matrix coupling elements is determined by the distance between the monomers and their relative orientation. The orientation of the transition dipoles is determined by the orientation of the monomers—hence the dipole-dipole interaction changes if the relative orientation of the monomers varies. This allows us to combine information obtained from absorption spectra and from CD spectra to gain information about the structure of the dimer, i.e., the relative orientation of the monomers. The asymmetry of the CD spectrum is in this case particularly helpful, because it will turn out that only for very few relative orientations does the spectrum show asymmetry at all. In this paper we only consider stick spectra. The issue of inhomogeneous broadening and the recovery of data from broadened spectra is extremely important for quantitative interpretations (Koolhaas et al., 1994, Somsen, 1995) and will be treated in a subsequent paper (Koolhaas et al., unpublished observations), but will not modify the conclusions drawn here. The organization of this paper is as follows: in the next section we introduce the model we use to calculate the spectra. In the subsequent subsections we classify various terms according to their effects on the CD spectrum. The third section is devoted to the application of the model to the B820 particle and the antenna systems LH1 and LH2, and the final section is devoted to remarks and conclusions. Most of the relevant mathematics can be found in the appendices.

THE EXCITONICALLY COUPLED DIMER MODEL

As stated in the Introduction, the usual way to treat the excitonically coupled dimer is to consider the monomers as two level systems, which are coupled through their transition dipole moments. This is even the case if more than one transition is taken into account: in that case each transition is supposedly independent of the others. The monomers exhibit a number of transitions, which are usually labeled as Q_y, Q_x, B_y, and B_x, starting from the lowest energy. Although the development in this and in the next section is completely general, we will illustrate most of the results for the B820, $\alpha\beta$ $BChl_2$ dimer. A list of numerical values for this system used throughout this paper is given in Table 1. Room temperature absorption and CD spectra of B820 are shown in Fig. 1.

As a consequence of the exciton coupling the dimer spectrum consists of a number of pairs of lines, and because

TABLE 1 Line positions and intensities of B820 in absorption and CD spectra*

Chang	At room temperature			
Absorp. max	Q_y	821 nm	Intensity	0.6
	Q_x	594 nm		0.18
CD max.	Q_y	816 nm	mol. ellipticity $\times 10^{-5}$	−1.04
	Q_y	776 nm		+0.50
	Q_x	609 nm		−0.13
	Q_x	587 nm		+0.12
Visschers	At T = 77 K			
Absorp. max	Q_y	825 nm	Intensity	0.6
CD max	Q_y	825 nm	mol. ellipticity $\times 10^{-5}$	−1.07
	Q_y	787 nm		+0.35
Fig. 1	At room temperature			
Absorp. max	Q_y	821 nm	Intensity	0.6
	Q_x	597 nm		0.13
CD max	Q_y	821 nm	$\times 10^4$	−6.3
	Q_y	783 nm		+3.2
	Q_x	613 nm		−0.3
	Q_x	592 nm		+0.9
Magnitude of the dipole moment	Q_y	6.3 D	Q_x	1.87 D

*As measured by Chang et al. (1990) and Visschers et al. (1991) and as shown in Fig. 1 (Frese et al., manuscript in preparation).

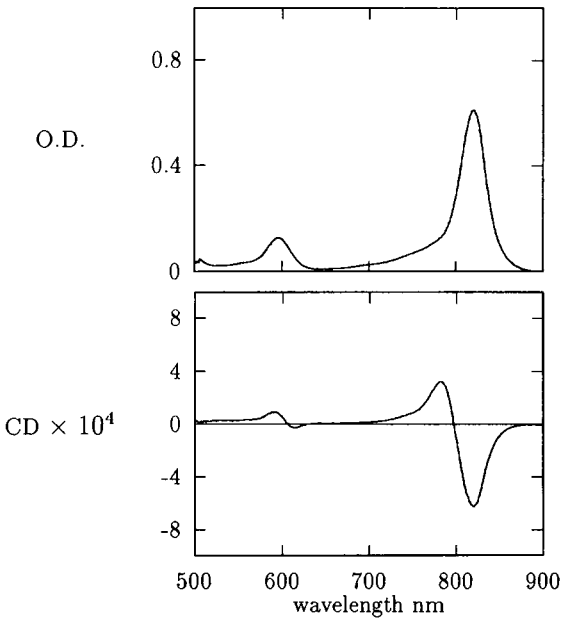

FIGURE 1 Room temperature absorption and CD spectra of the B820 subunit form of LH1 of *Rs. rubrum* (Frese et al., manuscript in preparation). The absorption and CD spectra were measured by means of a home-built spectrophotometer, using a opto-acoustic modulator (HINDS) and double lock-in technique (Ithaco 391A and EG&G 5209). A further description can be found in Van Mourik et al. (1990). The B820 subunit was isolated using a Superdex 200 column twice, so the reaction centers were removed completely. A further description can be found in Visschers et al. (1992). The sample was prepared in 50 mM phosphate buffer (pH 7.8) containing 0.6% *n*-octyl-beta-D-glucopyranoside (OGP) (Sigma Chemical Co.).

the distance between the monomers is such that the variation of the field intensity of the light is nonnegligible, a CD signal can also be measured.

In Appendix A we derive some general results for N-level systems; in this section we limit ourselves mainly to $N = 3$, restricting ourselves to the ground state and the Q_y and Q_x levels, although some of the possible effects of mixing with the B_y and B_x states will also be discussed, giving $N = 5$.

The central idea of this paper is that a nonconservative CD can only result from coupling of different transition moments. Strictly speaking, the CD spectrum as a whole is of course conservative, i.e., when summed over all of the lines, but as shown in Fig. 1, each of the pairs of lines can exhibit a pronounced asymmetry. On the basis of perturbation theory (cf. Appendix A) we conclude that in general the major contribution to the CD spectrum is from the (nearly) resonant transitions; in other words, the CD spectrum at the Q_y transition results from the coupling of the Q_y transition moments. This coupling gives a conservative contribution. However, the geometry of the system can be such that the rotational strength is small, or zero, in which case the nonresonant coupling will become measurable. As we will show in this section, the nonresonant couplings again give rise to a conservative spectrum, but with one line at the Q_x transition, whereas the other line is at the Q_y transition. Because the effects of both couplings are now on the same order of magnitude, each of the line pairs becomes asymmetrical. A direct implication of this is that asymmetrical CD lines are of weak intensity, as was observed experimentally by Kramer et al. (1984a). In addition, this has the interesting consequence that more definite conclusions can be drawn about the geometry of the dimer, or at least a suitable set of starting values can be given for a parameter search.

In this section we will look at the effects of various coupling terms for the three-level system. The starting point is the two-level system, in fact, two two-level systems in which only the y-y coupling and the x-x coupling are turned on, and the consequences of x-y coupling are then investigated. The geometry of the BChls used in our calculations is shown in Fig. 2.

The dimer Hamiltonian is given by

$$\mathcal{H} = \mathcal{H}_1 + \mathcal{H}_2 + \hat{V}, \tag{1}$$

where $\mathcal{H}_i$ are the monomer Hamiltonians and $\hat{V}$ denotes the interaction operator between the monomers, which, in the point dipole approximation, is given by

$$\hat{V} = \frac{1}{4\pi\epsilon R^3}\hat{\vec{\mu}}^1 \cdot \left(1 - 3\frac{\vec{R}\vec{R}}{R^2}\right) \cdot \hat{\vec{\mu}}^2, \tag{2}$$

where $\vec{R}$ is the vector connecting the centers of the monomers, i.e., the Mg atoms and $\hat{\vec{\mu}}^1$ and $\hat{\vec{\mu}}^2$ are the dipole operators of monomer 1 and monomer 2, respectively.

The molecular frame of the monomer is chosen such that the dipole moments of the Q_x and Q_y transitions are along the molecular x and y axes, respectively. (In reality, the transition moment may make small angles with the long and short axes of the molecule (Pearlstein, 1991).) We then have to refer all vectors in the expression for $\hat{V}$ to one and the same frame, for which we choose the molecular frame of monomer 1. The vector $\vec{R}$ is characterized by the polar angle θ and the azimuth ϕ in this frame, and the orientation of monomer 2 by its Euler angles α, β, and γ (Rose, 1957). The relation between the orientations of the monomers and the value of the interaction Hamiltonian is given in Appendix B.

In accordance with the notation of Appendix A, we denote the direct product states $|ij\rangle$, where now $i, j = 0, y, x$.

Coupled two-level systems

In this subsection we describe how, in principle at least, the relative position and orientation of monomers in a dimer can be obtained from the intensities and line positions of the Q_y and Q_x transitions. In the coupled two-level system there is only one coupling matrix element, which in the notation of Appendix A can be written as $V_{0y,y0}$, which of course depends on the above-defined angles and the distance R, six parameters in all. It is easy to show that if we also take into account the Q_x levels, but not the coupling between Q_x and Q_y, the couplings are independent in the sense that we get independent exciton splitting, and the (small second-order)

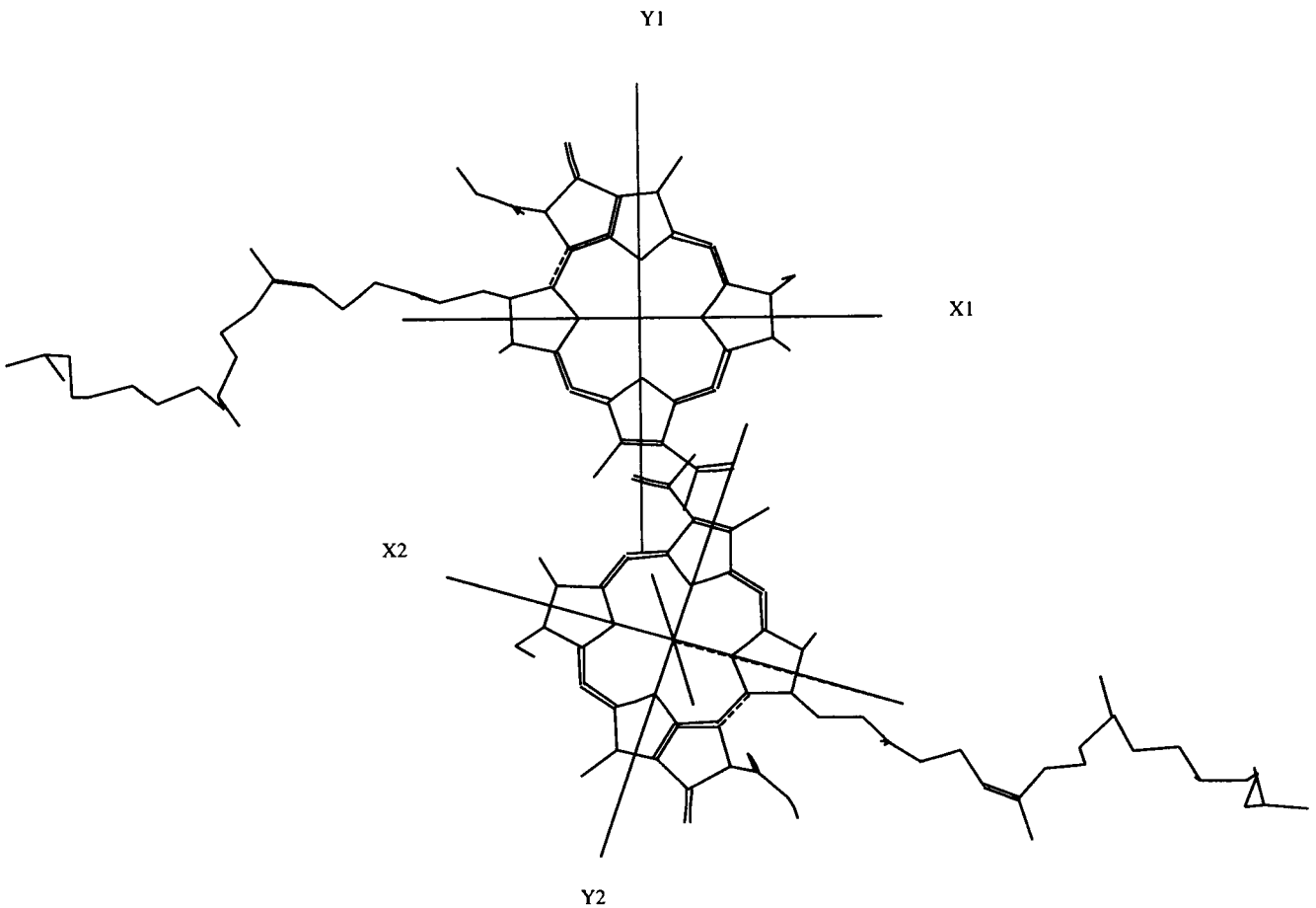

FIGURE 2 The arrangement of the BChls used in all calculations. The transition moments $\vec{\mu}_x$ and $\vec{\mu}_y$ are assumed to be along the x and y axes of the molecule, respectively. The molecular axes of molecule 1 are along the vertical and horizontal axes of the picture. The axes of molecule 2 are rotated and tilted. The small axis without a label is the z axis, which is perpendicular to the molecular plane. The Mg atom of molecule 1 is in the plane of the picture. The Mg atom of the other molecule is lifted toward the reader. Therefore $\vec{R}$ points slightly out of the plane. The same geometry is also given in Fig. 4; it corresponds to the points $D_yD_xD_R$.

effect on the ground state is strictly additive. The coupling between the Q_x levels is governed by the matrix element $V_{0x,x0}$. In Appendix C we give a short review of the diagonalization procedure and results for coupled two-level systems. Thus the following numbers can be obtained from the absorption and CD spectrum:

1. From the distance between the lines of one doublet, we get $V_{0y,y0}$ and $V_{0x,x0}$.
2. From the ratio of intensities of each doublet, we get $C^1_{y0}C^1_{0y}\cos\theta_{yy}$ and $C^1_{x0}C^1_{0x}\cos\theta_{xx}$. Here θ_{yy} is the angle between the Q_y transition moments, and θ_{xx} the angle between the Q_x transition moments. To obtain these results we also made use of the orthonormal properties of the matrix C^n_{ij} which couples the old and new states. These coefficients, in turn, depend in a well-known way on the coupling matrix element (cf. Appendix C).
3. From the rotational strength of both transitions we get $(C^0_{00})^2C^1_{y0}C^1_{0y}\vec{R}\cdot(\vec{\mu}^1_{0y}\times\vec{\mu}^2_{0y})$ from the Q_y transitions and $(C^0_{00})^2C^1_{x0}C^1_{0x}\vec{R}\cdot(\vec{\mu}^1_{0x}\times\vec{\mu}^2_{0x})$ for Q_x. Again, these depend on the V's, the above-defined θ's, and the angles between $\vec{R}$ and the cross-products, the length of $\vec{R}$, and the magnitudes of the transition dipole moments.

We therefore have six independent quantities that depend either directly on the six parameters referred to above or indirectly on the coupling matrix elements. This is sufficient to determine the angles and distance between the monomers by inversion. Analytical expressions are available for each of the quantities, and solutions can therefore be found from procedures described by Press et al. (1992).

In practice, the numbers referred to above cannot be obtained simply from measured spectra: the excitonic splitting may be too small to be observed, as in the Q_x transition of B820, and inhomogeneous broadening complicates recovery of the data.

Cross-coupling between different levels

The intensity of the CD lines is determined by two quantities: the coefficients C^n_{ij} and the angles between the transi-

tion moments. The coefficients are not small in most cases. For the degenerate dimers they are equal to $1/\sqrt{2}$ (cf. Appendix C) and in general are close to this value, so the reason for the general low-intensity rotational strengths measured in B820 is that the transition moments of the monomers are nearly parallel and/or in the same plane with $\vec{R}$. In this case other effects can be of relevance, and in this subsection we offer an explanation for the asymmetry of CD spectra.

First we look at a system in which only the *y-y* and the *x-x* couplings are turned on. This means that the nonzero coupling elements in the operator $\hat{V}$ are given by $V_{0y,y0} = V_{00,yy}$ and $V_{0x,x0} = V_{00,xx}$. The spectrum can be calculated, either by numerical diagonalization of the resulting Hamiltonian or by using the results of Appendix C. The angles and distances are published by Visschers et al. (1991). The values are given in Table 1. As is well established, both transitions give rise to a pair of lines in the absorption spectrum (Fig. 3 *A*), and the CD spectrum is conservative for each pair (Fig. 3 *B*).

Next, we turn off the contributions of the above-mentioned coupling terms to the CD spectrum, and consider only the coupling between Q_y and the Q_x transition, i.e., $V_{0x,y0}$ and similar terms. Note that the Q_y Q_y and the Q_x Q_x couplings that split the OD spectrum in the Q_x and Q_y regions, respectively, are still present; the Q_y Q_x couplings have hardly any effect on these splittings. This illustrates that the CD spectrum now consists of two pairs with opposite signs at the positions of the Q_y and the Q_x transitions. This is shown in Fig. 3 *C*.

The CD spectrum is the result of the combined effects. The asymmetry, although always present, only becomes visible when the effects are of comparable magnitude. As was stated earlier, for the *y-y* and the *x-x* couplings, the coefficients are close to $1/\sqrt{2}$. For the cross-coupling the magnitude of mixing of Q_x with Q_y will be on the order of $V_{0x,y0}/\Delta E$. The contributions of the Q_y Q_x dipole moments to the CD spectrum can only be comparable to the Q_y Q_y contribution if the latter is very small. The angle between the Q_y dipoles is small: the rotational strength is in that case proportional to sin θ_{yy}, for instance (cf. Eq. A.10), and/or the Q_y Q_y dipoles are (almost) in a single plane with $\vec{R}$. In addition, we note that the cross-coupling terms only give rise to an asymmetrical CD if $V_{0x,y0} \neq V_{0y,x0}$. This can also

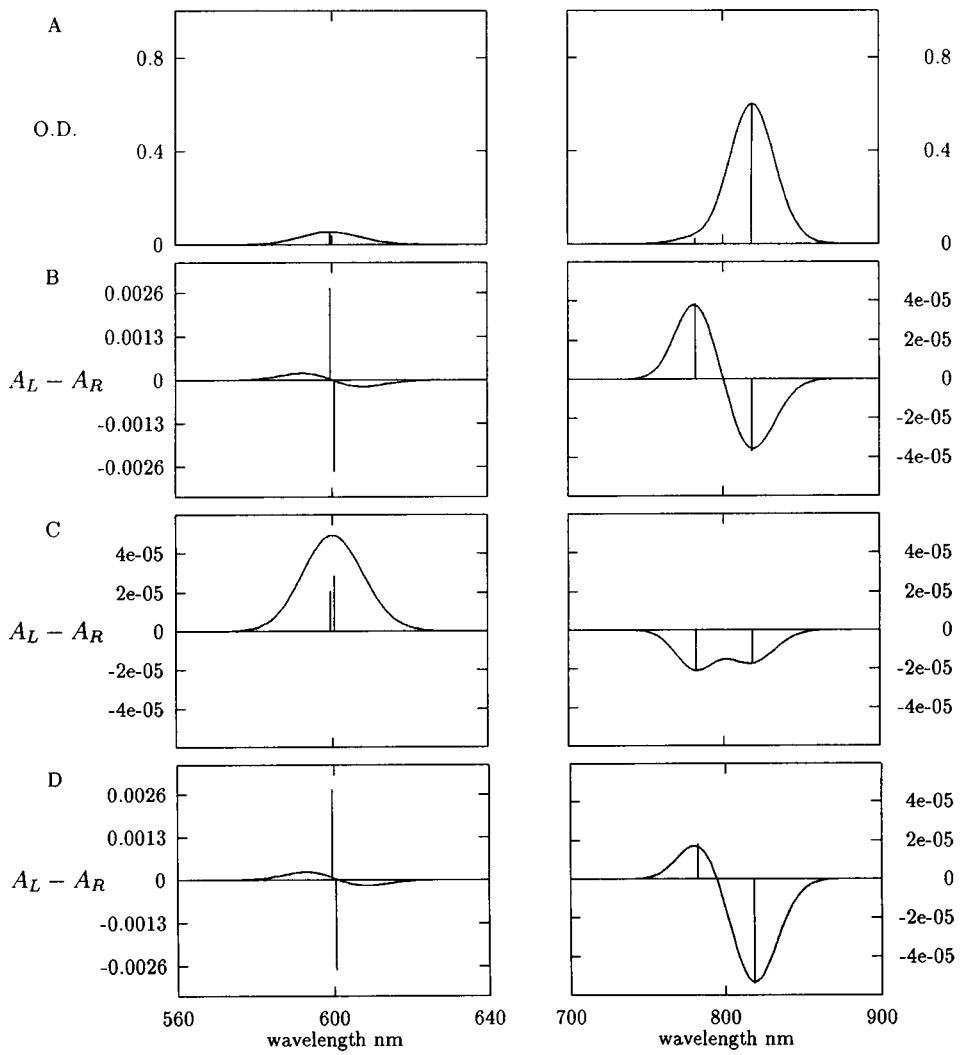

FIGURE 3 In all pictures the sticks are convoluted with a Gaussian to resemble spectra. (*A*) The calculated absorption spectrum of B820 in the Q_x and the Q_y areas, respectively. The CD spectrum is equal to the sum of contributions of resonant and nonresonant dipole transitions. The A_L-A_R spectra equal four times the rotational strength (cf. Eq. A.6). (*B*) The contributions of the resonant dipole moments to the CD spectrum. (*C*) The contributions of nonresonant moments to the CD spectrum. (*D*) The total CD spectrum. Note that the line splitting in the Q_x is very small. Therefore the intensity and the maxima in experimental spectra differ dramatically from stick spectra. In a forthcoming paper we will discuss line shapes to quantify this effect. Here we focus on the nonconservative character of the Q_y part of the spectrum. The magnitudes of the contributions of the resonant and the nonresonant moments are comparable; therefore the CD spectrum in the Q_y area is nonconservative.

be inferred from Eq. A.10: the coefficients C^n_{0i} and C^n_{i0} must be unequal, otherwise the sum makes the expression vanish.

If we put in the numbers given in Table 1 and Appendix A, we can give a rough estimate of the maximum angle between the y axes, for instance, $V_{0x,y0}/\Delta E \approx 0.02$. Assuming that we need at least a 10% contribution to observe the asymmetry, that means that $\sin \theta_{yy} < 0.2$, and consequently that the angle between the y axes is less than about 20°. The real peak ratio is 1:−3 at 77K. That implies a contribution due to $\vec{R} \cdot (\vec{\mu}^1_{y0} \times \vec{\mu}^2_{0x})$ and similar terms as large as ½ times the contribution of $\vec{R} \cdot (\vec{\mu}^1_{y0} \times \vec{\mu}^2_{0y})$.

The CD spectrum in the region from 550 to 650 nm is also nonconservative (Fig. 1). The contribution of $\vec{R} \cdot (\vec{\mu}^1_{x0} \times \vec{\mu}^2_{0x})$, however, dominates the stick spectrum, but in the experimentally obtained spectrum this contribution is almost canceled by the enormous overlap of the broadened lines because of a very small line splitting. As we do not discuss line shapes, we focus on the symmetry of the Q_y transition, which results from the orientation of the monomers.

In principle, the information about the angles between the transition moments can of course be obtained from the ratio of intensities of the absorption spectrum, as was indicated above. In practice, inhomogeneous broadening makes such information unobtainable, as can be seen, for instance, from the spectrum in the Q_x transition region. The CD spectrum still clearly exhibits the fact that there are two transitions.

FURTHER ANALYSIS OF THE DIMER STRUCTURE

As was shown in the previous section, analysis of spectra can lead to reductions in the available parameter space of the possible geometries of molecules in a complex. In this section we will deduce limits for the possible structure of the B820, $\alpha\beta$ $BChl_2$ subunit, which is a part of the LH1 light-harvesting antenna, and of a (fictitious) dimer occurring in the LH2 complex.

We will argue, on the basis of the similarity of the spectra of B820 and LH1, that the structure of the dimer in the LH1 complex, which is an aggregate of B820 particles, is close to the structure of the dimer in the B820. Using this similarity, we derive the spectrum of a fictitious particle "B850" derived from the known structure of LH2 (McDermott et al., 1995). Comparison of these structures leads to the conclusion that the arrangement of the BChl in the LH1 complex differs considerably from that of LH2, as is to be expected based on the differences in the CD spectra. The spectra of LH1 and B820 are very nonconservative, whereas the CD spectrum of LH2 is clearly conservative.

In this paper the analysis is restricted to degenerate molecules. In the case of nondegenerate molecules, more parameters are introduced into the problem. This is a complex issue, because the interaction with the surroundings is responsible for this nondegeneracy. In that case additional spectroscopic information (for instance, fluorescence anisotropy of linear dichroism) must be used to unambiguously determine the structure (Koolhaas et al., 1994; Cantor and Schimmel, 1980; Craig and Thirunamachandran, 1984).

Although we base our analysis on stick spectra, most of the calculated spectra shown are convoluted with a Gaussian line shape, to make them resemble true spectra. This has a marked effect on the positions of the lines, particularly in the case of CD spectra (Somsen et al., 1996). Other models that reproduce the shape of absorption and CD lines, such as the diagonal disorder model (Koolhaas et al., 1994), give similar results, although the abstracted parameters for different models can be quite different. A detailed discussion of the role of inhomogeneous broadening on CD spectra of pigment-protein complexes is the subject of a subsequent paper (Koolhaas et al., unpublished observations).

The absorption spectrum

The analysis of the absorption spectrum is discussed in the previous section. Here we summarize the results.

The absorption spectrum is dominated by the contributions of resonant transition moments. The line positions and intensities are directly related to the dipole-dipole interaction matrix element and the angle between the monomeric dipole moments, respectively, and accuracies of the derived values are directly related to the distinctness of features in the spectrum. The angle between the dipole moments, for instance, cannot be resolved at all from spectra with little structure, such as the Q_x region of B820.

The outcome of our analysis is represented in Fig. 4. All coordinates are given in the molecular frame of monomer 1. In this coordinate frame we draw the vectors $\vec{R}$, and the dipole transition moments of monomer 2, which in this section are given without their superscript, $\vec{\mu}_x$ and $\vec{\mu}_y$. Thus we find for $\vec{\mu}_y$ that it must lie on a cone around the y axis. Because all expressions are invariant for inversion of the monomer dipole moments, the xz plane of the figure is a plane of reflection, and the spectrum is invariant for inversion around the origin of both the transition dipole moments and the vector $\vec{R}$.

The resulting cones are indicated by the second circles from the bottom and the top in Fig. 4, on which the points with subscript y are marked. The two large circles in this figure then give the limits between which $\vec{\mu}_x$ must be positioned.

The CD spectrum

We showed in the second section that the positions of the lines in the CD spectrum depend mainly on the resonant interactions between the monomers; nonresonant contributions have a negligible effect. This is not true for the intensities, however. For particular arrangements of the monomers, the rotational strength due to the resonant contributions can well be zero, and only the nonresonant parts contribute asymmetrically to different parts of the spectrum.

From the positions of the peaks in the CD spectrum, we again find the cones around the y axis on which $\vec{\mu}_y$ must be positioned, but because the CD spectrum also shows the two

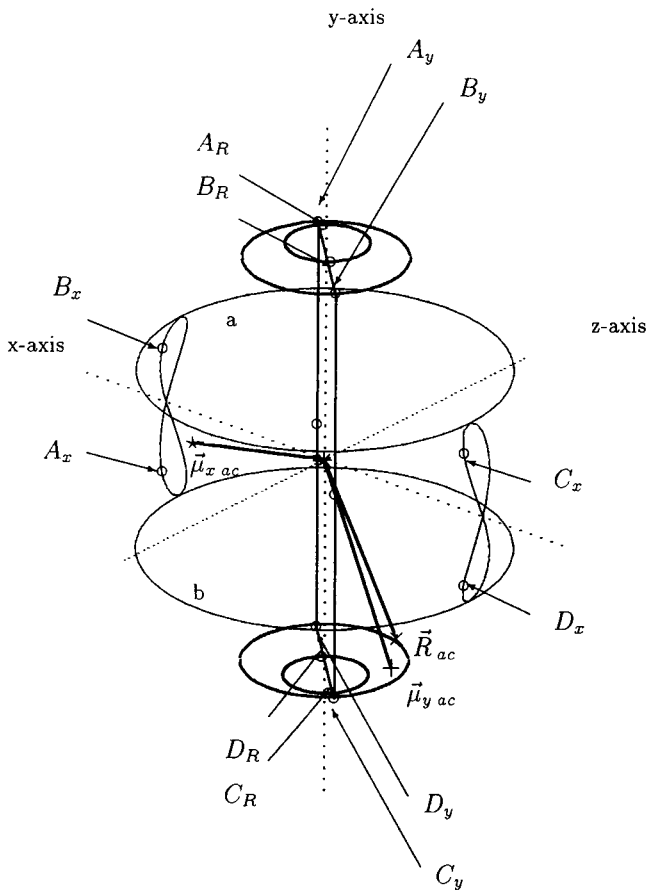

FIGURE 4 The axes in the figure correspond to the molecular axes of monomer 1, with the Q_x (and B_x) transitions along x, and the Q_y (and B_y) transitions along y. As described in the text, the position and orientation of the second monomer of B820 are given by the following: $\vec{\mu}_y$ is either on the circle labeled A_yB_y or on C_yD_y, $\vec{R}$ is either on the circle A_RB_R or on C_RD_R, and $\vec{\mu}_x$ is somewhere on or between the curves a and b. In addition, the y axis, $\vec{\mu}_y$, and $\vec{R}$ are (almost) in one plane. A possible choice, giving the correct intensity ratios and line positions, is the plane denoted $A_yB_yC_yD_y$. In view of the symmetry relations also described in the text, only the orientations C_yC_R or D_yD_R are possible. The meaning of the 8-shaped curves is discussed in the text; they lead to symmetry relations of the transition moments. The geometry denoted by the points $D_yD_RD_x$ is the one given in Fig. 2 and is used in all subsequent calculations. Also shown are the positions and orientations of monomer 2 of a dimer in the LH2 complex of *Rps. acidophila*, based on the known structure. This structure corresponds to the vectors labeled $\vec{R}_{ac}$, $\vec{\mu}_{y\,ac}$, and $\vec{\mu}_{x\,ac}$.

separate peaks in the Q_x region, whereas the absorption spectrum does not, we can put more severe limitations on the orientation of $\vec{\mu}_x$. This would lead to cones around the x axis, with corresponding large circles parallel to the yz plane. On the other hand, the positions of the sticks in the CD spectrum are extremely sensitive to the model used to generate the broadened spectrum (Koolhaas et al., 1994; Somsen, 1995; Koolhaas et al., unpublished observations), so one has to be careful here.

The vector $\vec{R}$ plays a more prominent role in the CD spectrum than in the absorption spectrum: the rotational strengths are linear in R. The invariance properties are also different: only inversion of $\vec{\mu}_y$ and $\vec{R}$ simultaneously (or $\vec{\mu}_x$ and $\vec{R}$) now leads to the same spectra.

For nonconservative CD spectra the resonant contribution must be small. This means that the angle between the monomer transition dipole moments must be small or that $\vec{R}$ is almost in the same plane as these dipole moments, or a combination of both. Analysis of the absorption spectrum yields the angle between the resonant moments. In the case of a pronounced asymmetry and an angle between the resonant moments larger than about 20°, the second possibility, $\vec{R}$ in or close to the plane of the y axis and $\vec{\mu}_y$ is the only remaining option. The relative contributions of the conservative and the nonconservative parts can be deduced from the peak ratio, because they are additive.

The small circles at the top and bottom of Fig. 4 give the possible orientations of the vector $\vec{R}$.

The B820 particle of *Rs. rubrum*

We now proceed to deduce the geometry of the BChl dimer in B820. The basic information obtained from spectra measured by Visschers et al. (1991) and by Chang et al. (1990) is given in Table 1.

The measured CD spectra of B820 are clearly nonconservative in the Q_y region, from 700 to 950 nm. The peak ratios are not equal: Visschers measured the ratio 1:−3 at 77K. At room temperature the peak ratio observed by Chang (shown in Fig. 1) is 1:−2 (Frese et al., manuscript in preparation). This difference could be the result of the different temperatures at which the measurements were made, and it could indicate a slight structural shift as a function of the temperature. As long as measurements on one and the same sample at different temperatures and on the same apparatus are not available, it is hard to draw definite conclusions regarding such changes in structure. The CD spectrum measured by Chang et al. (1990) shows an unusual shift in the peak positions. This shift can be caused by the experimental setup or by the presence of some reaction center complexes. The intensities in the CD spectrum are dependent on the line shapes. Therefore, at this point we estimate the length of $\vec{R}$ to be equal to $R = 1.1$ nm, and analysis of the available data then yields an angle of about 16° or (180 + 16)° between $\vec{R}$ and the $\vec{\mu}_y$. In the forthcoming paper the magnitude of $\vec{R}$ will be deduced.

The value of the angle between $\vec{\mu}_y^1$ and $\vec{\mu}_y^2$ was stated by Visschers to be 24° or (180 − 24)° on the basis of their absorption and polarized fluorescence excitation measurements (Visschers et al., 1991). As we argued in the previous subsection, this implies that the vector $\vec{R}$ must be almost coplanar with $\vec{\mu}_y^1$ and $\vec{\mu}_y^2$. The CD signals are very sensitive to small changes in this angle. We show the change in the ratio of the CD signals as a function of the angle of $\vec{R}$ with the above-mentioned plane of the Q_y moments in Fig. 5. The orientations of the molecular planes do not change from those depicted in Fig. 2; only the position of one BChl is varied.

Analysis of the data yields the points A_y, B_y, C_y, and D_y in Fig. 4 for the possible location of $\vec{\mu}_y$, as giving the correct

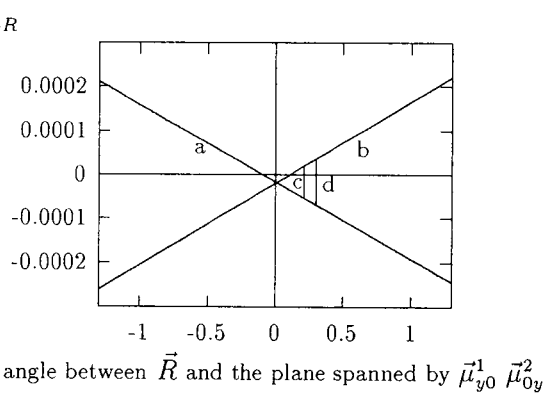

FIGURE 5 The total intensity of the CD signal at 820 nm and at 780 nm while the direction of $\vec{R}$ is varied with respect to the plane spanned by the Q_y transition moments. At zero degrees all three vectors are in one plane, and at that point the CD intensity arises solely from the coupling between Q_x and Q_y transitions. Label *a* represents the intensity of the line at 820 nm. Label *b* represents the intensity of the line at 780 nm. The line near label *c* denotes the angle when the peak ratio of the lines at 780:820 is equal to 1:−3. The angle between $\vec{R}$ and the plane is 0.2°. The ratio is 1:−2 at label *d*. The angle at label *d* is 0.3°.

line positions and intensity ratios. The vector $\vec{R}$ must be on one of the small circles A_R B_R or C_R D_R in this figure and close to the plane through points A_y, B_y, C_y, and D_y. The signs of the CD lines further restrict the orientations of $\vec{R}$ to the same side of this plane as $\vec{\mu}_y$. Thus, for instance, if we choose A_y for the $\vec{\mu}_y$ orientation, we must have A_R for $\vec{R}$.

The orientation of $\vec{\mu}_x$ is limited by the large circles in Fig. 4. A further reduction of the available parameter space for $\vec{\mu}_x$ can be achieved by combining the signs of the CD signals in the Q_x area and the peak ratio in the Q_y region. To illustrate how this reduction takes place we consider how $\vec{\mu}_x$ changes when we let $\vec{\mu}_y$ go around the circle defined by the points A_y and B_y. Although in general three rotations are needed to obtain an arbitrary orientation of the molecular coordinate frame of monomer 2 with respect to the frame monomer 1 (Rose, 1957), we can get the *y* axis of monomer 2 on any point of the circle by just two rotations: a rotation around the *z* axis of monomer 1, followed by a rotation around its *x* axis. This procedure limits the orientation of the *x* axis of monomer 2 to the 8-shaped curve, labeled by A_x and B_x, in Fig. 4.

By a similar procedure, now moving the *y* axis of monomer 2 around the circle at the bottom of the figure, the curve labeled with C_x and D_x is obtained. Note, however, that this is not the inversion image of the first curve: the points C_x and D_x are at the same side of the *xy* plane as A_x and B_x.

The CD spectrum in the Q_y region gives the correct peak ratio 1:−3 for the points C_yC_x and D_yD_x; for the orientations A_yA_x and B_yB_x the peak ratio in the Q_y region is the opposite, i.e., −1:3. Using a model to calculate the line shapes, it would also be possible to discriminate between the orientations C_yC_x and D_yD_x by comparing the ratio of the CD signals in the Q_y versus the Q_x regions, as will be done in the forthcoming paper. Then the only remaining symmetry property is the inversion symmetry of all vectors, i.e., $\vec{R}$ as well as the transition dipole moments simultaneously.

The absorption and CD spectra of B820 have been analyzed on the basis of two interacting three-level model systems. One remaining question is what the effects of the other transitions, commonly denoted as B_y and B_x, are. As can be inferred from the above analysis, the effects on the absorption spectra in the Q_y region must be small. But the effect on CD spectra cannot be neglected. Using the same argument as at the end of the second section, we note that the energy difference between the B_x and Q_y transition is much larger than between Q_x and Q_y (the B_x transition is at approximately 350 nm), but the B_x transition dipole moment (9.3 D) is much larger than the Q_x moment, and consequently the perturbation effect of B_x on Q_y is approximately on the same order of magnitude as the effect of Q_x on Q_y. It is not hard to include these effects numerically as well. This changes the maximum angle between $\vec{R}$ and the $\vec{\mu}^1_y - \vec{\mu}^2_y$ plane to about 2° rather than less than 1°.

The main conclusion, that the vectors $\vec{\mu}^1_y$, $\vec{\mu}^2_y$, and $\vec{R}$ are (almost) in one plane, remains valid. The effect of the B_x transition on the CD spectrum in the Q_y region is on the same order of magnitude as the effect of Q_x. The sensitivity of the asymmetry to a small variation in the angles remains valid: the effects are additive in a perturbation approach, which we claim is sufficient for these couplings.

A slight variation in the vector $\vec{R}$ with respect to the plane determined by the monomer *y* axes changes the peak ratio of nonconservative CD spectra considerably. Even at room temperature these vectors maintain this specific orientation.

Comparison of the geometry of the B820 dimer with LH1 structure

LH1 is one of the light-harvesting complexes used by purple bacteria to collect solar energy. The spectroscopy of the complex as well as its organization are not fully understood. Karrasch et al. (1995) have obtained the structure of LH1 of *Rs. rubrum*, with a resolution of ~8.5 Å. The authors claim LH1 to be a ring of 16 $\alpha\beta$ subunits. Each unit binds two BChla molecules and is thought to be similar to the B820 particle (Visser et al., 1995). This resolution, however, is not sufficient to establish the arrangement of the BChls within the complex. To understand the geometry of the BChls in LH1 it is interesting to compare the spectroscopic features of LH1 with the spectra of B820.

The absorption spectrum of LH1 of *Rs. rubrum* (Kramer et al., 1984a) is shifted with respect to B820, and at room temperature the maximum is at 875 nm. The CD spectrum of LH1 of *Rs. rubrum* (Kramer et al., 1984a) is shifted as well. The lines in the Q_y region, from 700 to 950 nm, are clearly nonconservative, with a peak ratio of 1:−1.6 at 77K, whereas the peak ratio of B820 was 1:−3 at that temperature (Visschers et al., 1991). On the other hand, for LH1 of *Rhodobacter sphaeroides*, fully nonconservative CD spectra can be observed in the Q_y region (Frese et al., manuscript in preparation). This spectrum looks rather similar to the calculated spectrum depicted in Fig. 3 *C*.

If we ascribe the spectroscopic features of LH1 to a BChl dimer, the change in the geometry in B820 upon formation of the ring structure of LH1 can be quantified. The shift of the LH1 absorption spectrum relative to B820 is attributed to a lowering of the first excited state, the Q_y energy level of the BChl monomers, due to its large polarizability, as was measured by Beekman et al. (manuscript to be submitted). The height of the Q_x energy levels remains unchanged. The dimer of the two such BChl molecules used to calculate the spectroscopic features of LH1 is subsequently referred to as the LH1 dimer.

This shift of the Q_y energy makes the CD spectrum somewhat more conservative at the same geometry, as a consequence of the larger energy difference between the two lowest excited states. The asymmetry is calculated to be $1:-2.2$ if the LH1 dimer has the same geometry as B820. A further reduction of the peak ratio from $1:-2.2$ to the measured $1:-1.6$ could be caused by a change in the geometry of the LH1 dimer. In view of our calculations in the previous subsection, this change must be very small. Moving the vector $\vec{R}$ away from the plane spanned by the vectors $\vec{\mu}_y^1$ and $\vec{\mu}_y^2$ by much less than a degree is sufficient to explain this change (cf. Fig. 5).

We can thus conclude that the spectroscopy of LH1 can be understood by using a dimer model and that the change in geometry in the B820 dimer upon ring formation is very small; the Q_y transition moments $\vec{R}$ are (almost) in one plane, the plane of the ring.

Comparison of the geometry of the LH1 dimer with the dimer of the B850 band of LH2

We can turn the argument of the previous section around and consider the spectroscopy of a fictitious dimer derived from a known antenna complex structure. The structure of LH2 of *Rps. acidophila* was obtained by McDermott et al. (1995) with a resolution of 2.5 Å. The pigments in LH2 are shown to be arranged on two rings. One ring consists of nine BChl monomers absorbing primarily at 800 nm. The other ring, absorbing at 850 nm, is formed by nine BChl dimers. Each dimer is bound to an α and a β polypeptide. We subsequently call the two BChls bound to an $\alpha\beta$ pair a LH2 dimer. The spectroscopic properties of this LH2 dimer can be calculated using the coordinates of this unit in LH2. The spectroscopic properties of neighboring BChls that are closest together are pictured in Fig. 6.

The absorption spectra of the LH1 dimer and the LH2 dimer are rather similar. The line-splitting in the Q_y region is slightly larger in the LH2 dimer, because of a smaller distance between the chromophores in LH2. The calculated absorption spectrum of the LH2 dimer and the measured LH2 spectrum are also similar.

The calculated CD spectrum of the LH2 dimer in the Q_y region is clearly conservative, as was experimentally observed (Cogdell and Scheer, 1985), but the position of the zero crossing in the calculated spectrum is on the blue side of the absorption maximum instead of on the red side, as in the experimentally obtained spectrum. The conservative nature of the calculated CD spectrum of the fictitious LH2 dimer is markedly different from that of the LH1 dimer. The reason, of course, is geometrical: we marked the geometry of the LH2 dimer in Fig. 4. This shows that the angle between the Q_y transition moments in LH2 dimer (McDermott et al., 1995) differs by a few degrees from the angle in B820 (Visschers et al., 1991); $\vec{R}$, however, is much farther away from the plane spanned by $\vec{\mu}_y^1$ and $\vec{\mu}_y^2$ than it is in the case of the LH1 dimer. The angle between $\vec{R}$ and this plane is now approximately 13°, leading to a much larger resonant contribution in the CD spectrum in the 700–950-nm region.

The spectroscopic features of two neighboring BChls of the B850 band, located on different subunits with a larger intermolecular distance than in the LH2 dimer, are very similar to the LH2 dimer. The CD spectrum is also conservative, although the amplitudes are smaller and the phase in the Q_y region of the spectrum is reversed. The angle of $\vec{R}$ with the plane spanned by $\vec{\mu}_y^1$ and $\vec{\mu}_y^2$ is the same, 13°. The positions of the lines in the absorption and CD spectra are closer together, as was found in case of the LH1 dimer. The angles between the Q_y dipole moments differ by a few degrees.

The spectroscopic features of the LH2 complex are not completely explained by a dimer model, the positions of the lines in the experimentally obtained CD spectrum and the calculated dimer spectrum are not identical (Sauer et al., 1996), but both LH2 and the LH2 dimer CD spectra are conservative. We conclude on the basis of the structure of LH2 not only that the calculated spectra of the LH2 dimer and the analysis of the spectroscopic features of LH1 that the ring structures of LH1 in *Rs. rubrum* and LH2 in *Rps. acidophila* differ in size, but that the relative orientations of the BChls in the two antenna systems differ as well.

REMARKS AND CONCLUSIONS

We have shown how the combined analysis of absorption and CD spectra can lead to a more or less unique geometrical structure (apart from overall inversion symmetry) of a dimer. In the simplest case, a degenerate dimer of three-level systems, these spectra are sufficient in principle, especially when the CD spectrum is nonconservative.

Obviously systems are more complicated than that in reality, and in addition, a model for the line shapes is necessary to gather the information needed to determine the geometry of the dimer. Moreover, there are parameters that are completely unknown, such as excited-state transition moments. Preliminary calculations, using different models for the line shapes (Koolhaas et al., unpublished observations), show, however, that in the case of nonconservative CD spectra, the conclusion that the resonant contribution is small and hence the transition moments are virtually in one plane with the vector $\vec{R}$, remains valid.

Other forms of spectroscopy may be needed here. For instance, in the case of nondegenerate monomers, fluores-

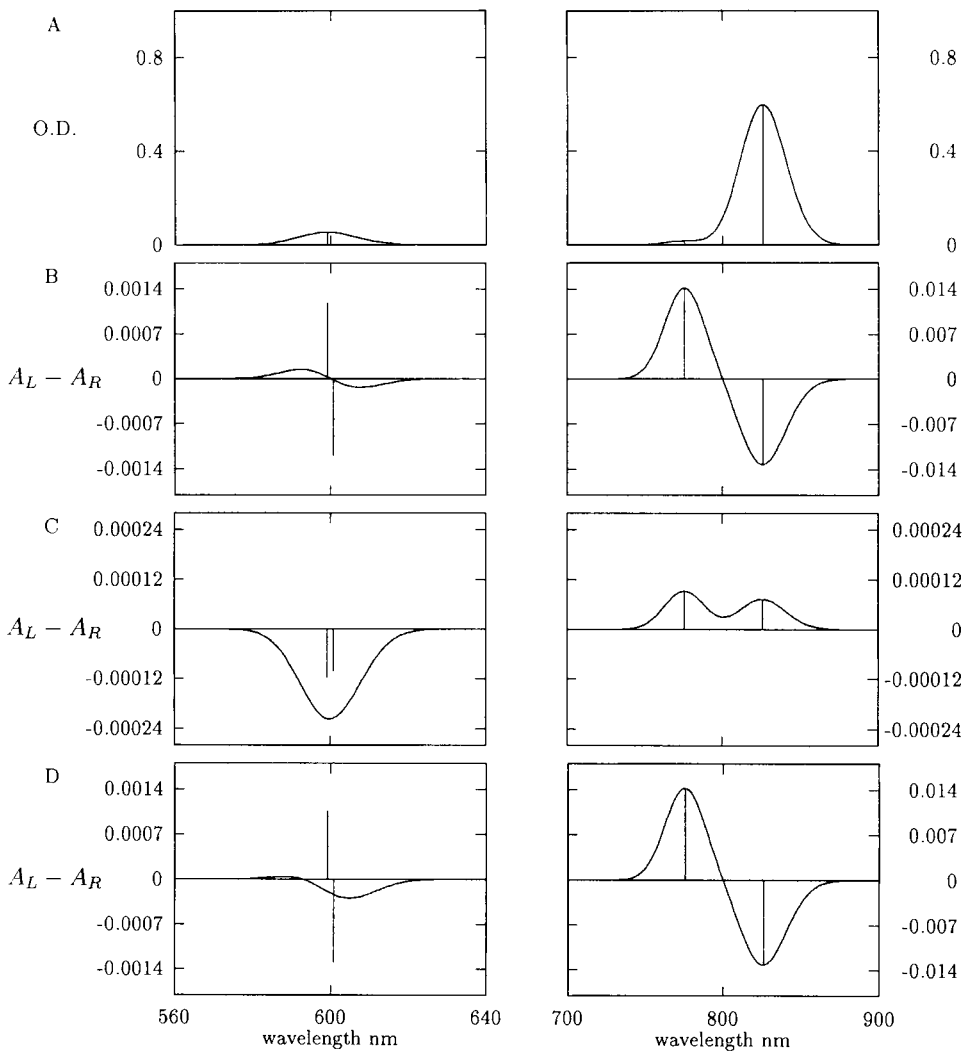

FIGURE 6 These spectra are a prediction of the spectroscopic properties of the LH2 dimer. They are obtained by using the coordinates of a dimer of BChls in the B850 band bound to the same subunit in LH2 of *Rhodopseudomonas acidophila*. (*A*) The absorption spectrum. (*B*) The contributions of resonant moments to CD spectrum. (*C*) The contributions of nonresonant moments to CD spectrum. (*D*) The total CD spectrum. This figure should be compared to Fig. 3. The contributions of the nonresonant moments to the Q_y part of the spectrum are clearly smaller than those of the resonant moments in contrast to B820; therefore the CD spectrum of the LH2 dimer is conservative in the region from 700 to 900 nm. The opposite holds for the Q_x part. This part is quite similar to B820. Finally, we note the different sign for the nonresonant contribution.

cence anisotropy measurements can be helpful for resolving the extra parameters. Changes in ground- and excited-state energies due to interaction of ground- and excited-state dipole moments with the surroundings could be resolved using Stark spectroscopy.

On the basis of our calculations in this paper, we can draw several conclusions that appear to remain valid if we use different models for the line shapes, turn on (arbitrary chosen) transition moments between excited states, include transitions to higher energy levels, such as the *B*-states, or, in the antenna systems, turn on the interaction with more monomers.

These conclusions are

- The structure of the B820 dimer is rather specific. The Q_y dipole moments and $\vec{R}$ are (almost) in one plane; even if we change the temperature from 77K to room temperature, the corresponding change in intensity ratio of the CD spectrum can be explained by minor changes in geometric arrangement. This implies that the monomers in the dimer are either tightly bound together, or that the surrounding protein limits the motion of the monomers considerably, even at higher temperatures.
- The absorption and CD spectra of LH1 can be understood by using a dimer model. The change in intensity ratio upon going from B820 to the LH1 complex of *Rs. rubrum* is also minor. The spectrum is shifted by a considerable amount, but the nonconservative nature of the CD spectrum is preserved, and although the shift in energies also has its influence on the CD spectrum, we can conclude that the LH1 dimer does not structurally differ much from B820.
- The arrangement of the chromophores in LH2 and the deduced geometry in LH1 differ. The angle between the Q_y transitions and $\vec{R}$ is much larger in LH2 than in LH1, causing a conservative CD spectrum. The angles between the Q_y transition moments are similar. We note that the positions of the lines in the absorption and the CD spectra of LH2 cannot be understood by using a degenerate dimer model.

APPENDIX A: COUPLED *N*-LEVEL SYSTEMS

In this appendix we give the expressions necessary to calculate the absorption and CD spectrum for two coupled *N*-level systems. We denote the

states of monomer i ($i = 1, 2$) by $|i; n\rangle$ and the corresponding energies by E_n^i. The monomer Hamiltonian can then be written as

$$\mathcal{H}_i = \sum_{n=0}^{N-1} E_n^i |i; n\rangle\langle i; n|. \tag{A.1}$$

The monomer transition dipole moments are denoted by

$$\vec{\mu}_{nm}^i = \langle i; n|\hat{\vec{\mu}}|i; m\rangle, \quad i = 1, 2. \tag{A.2}$$

A basis in the Hilbert space of dimer states is given by direct products of monomer states: $|nm\rangle = |1; n\rangle \otimes |2; m\rangle$. A typical matrix element of $\hat{V}$ (Eq. 2) can be written as

$$V_{nm,n'm'} = \langle nm|\hat{V}|n'm'\rangle = \frac{1}{4\pi\epsilon R^3}\vec{\mu}_{nn'}^1 \cdot \left(1 - 3\frac{\vec{R}\vec{R}}{R^2}\right) \cdot \vec{\mu}_{mm'}^2 \tag{A.3}$$

where we used the above definitions of product states and transition dipole moment elements.

Obviously the above introduced direct product states are not eigenstates of the dimer Hamiltonian. The new eigenstates, denoted by $|n\rangle$, are found by diagonalizing the Hamiltonian given in Eq. A.3 and are linear combinations of the old states:

$$|n\rangle = \sum_{i,j=0}^{N-1} C_{ij}^n |ij\rangle. \tag{A.4}$$

We consider only excitations from the ground state, now denoted by $|0\rangle$. Thus the absorption intensity for the transition $0 \rightarrow n$ is proportional to the transition dipole moment squared:

$$I_n \propto |\langle 0|\hat{\vec{\mu}}_1 + \hat{\vec{\mu}}_2|n\rangle|^2 = \left|\sum_{i,j,i'=0}^{N-1} [C_{ij}^0 C_{i'j}^n \vec{\mu}_{ii'}^1 + C_{ij}^0 C_{ji'}^n \vec{\mu}_{ii'}^2]\right|^2. \tag{A.5}$$

The intensity of the CD line is proportional to the so-called rotational strength R_n of the transition, which can be written as (Somsen, 1995)

$$R_n = \frac{\pi}{2\lambda_n}\sum_{i,j,i'=0}^{N-1}\sum_{k,l,k'=0}^{N-1} C_{ij}^0 C_{kl}^0 [C_{i'j}^n C_{lk'}^n (\vec{\mu}_{ii'}^1 \times \vec{\mu}_{kk'}^2) + C_{ji'}^n C_{k'l}^n (\vec{\mu}_{kk'}^1 \times \vec{\mu}_{ii'}^2)] \cdot \vec{R} \tag{A.6}$$

where λ_n is the wavelength corresponding to the excitation energy. $\vec{R}$ is defined as $\vec{R} = \vec{R}_2 - \vec{R}_1$.

The magnitude of the interaction Hamiltonian is primarily determined by the number

$$\mathcal{V} = \frac{\mu^2}{4\pi\epsilon_0 R^3} = 5.035\ \text{cm}^{-1} \quad \text{for} \quad \mu = 1\text{D} \quad \text{and} \quad R = 1\ \text{nm}, \tag{A.7}$$

where μ is the magnitude of the transition dipole moment. Typical values range from 1 to 10 D. Typical distances between the monomers are on the order of 1 nm, so that the numerical value (in wavenumbers) of this constant is between 5 and 500 cm^{-1}. The electronic transitions have energies of 10^4 cm^{-1} or higher. All of our calculations where performed by diagonalizing the Hamiltonian, but to understand the results it is instructive and sufficient, in view of the above numbers, to take the perturbative approach.

Although there are in principle $N^2 - N$ nonzero interaction matrix elements, assuming that none of the states have permanent dipole moments, only a few are experimentally available. From ground-state absorption experiments one only has access to the magnitude of the transition moments from the monomer ground state to the monomer excited state μ_{0k}^i. The directions of the transition moments are "coupled" to the molecular frame, i.e., the orientation of the frame determines these directions.

In a perturbation expansion scheme, the new states are found from the old states by the following expression:

$$|ij\rangle_{new} = \sum_{w \neq ij} \frac{\langle w|\hat{V}|ij\rangle_{old}}{E_w - E_{ij}}|w\rangle, \tag{A.8}$$

where the sum is over the old states. The magnitudes of the matrix elements are all determined by $\mathcal{V}$, but by far the largest contribution to the new states comes from states that are resonant or nearly resonant with the state considered. However, it is shown in the main body of the paper that the asymmetrical CD results if the geometry of the system is such that the vectorial products of the transition moments and distance vector are nearly zero. The nonresonant contributions then give rise to a weak, nonconservative CD. This means that we cannot a priori exclude transitions from excited states on the basis of magnitude of the matrix elements; however, numerical calculations where these states are included show only minor effects on the CD spectrum. Thus in the remainder of this paper we only take excitations from the ground state into account.

This means that Eqs. A.7 and A.8 reduce to

$$I_n \propto \left|\sum_{i,j=0}^{N-1} C_{0j}^0 [C_{ij}^n \vec{\mu}_{0i}^1 + C_{ji}^n \vec{\mu}_{0i}^2]\right|^2 \tag{A.9}$$

and

$$R_n = \frac{\pi}{\lambda_n}(C_{00}^0)^2 \sum_{i,j=0}^{N-1} C_{i0}^n C_{0j}^n (\vec{\mu}_{0i}^1 \times \vec{\mu}_{0j}^2) \cdot \vec{R}. \tag{A.10}$$

These two equations form the basis of most of our considerations of the second section. We note that the values of the absorption intensity and the rotational strength depend on the magnitude of the coefficients C_{ij}^n and on the relative orientations of the transition dipole moments and the vector $\vec{R}$. Relations between the orientations, the magnitude of the interaction matrix elements and of the absorption intensity, and rotational strengths are derived in the next appendix.

As a final remark, we note that the CD spectrum as a whole is strictly conservative. In other words the following relation does hold:

$$\sum_n R_n = 0, \tag{A.11}$$

or, if we take all rotational strengths originating from the ground state, these add up to zero. Because of the coupling between different levels, this is not the case for each pair of lines.

APPENDIX B: ORIENTATION AND DIPOLAR INTERACTION

In this appendix we give the elements of the interaction Hamiltonian $\hat{V}$ (cf. Eq. A.4) in terms of the relative orientation of the monomers. We must refer to all vectors in the expression for $\hat{V}$ to one and the same frame, for which we choose the molecular frame of monomer 1 (cf. the second section, The Excitonically Coupled Dimer Model).

Inner products of two vectors $\vec{a}$ and $\vec{b}$ can be expressed in terms of their spherical components in the following way (Rose, 1957):

$$\vec{a} \cdot \vec{b} = \sum_{m=-1}^{1} (-1)^m a_m b_{-m}, \tag{B.1}$$

and the spherical components themselves can be transformed between frames using the Wigner rotation matrices $D^{l}_{mm'}(\alpha, \beta, \gamma)$, according to

$$a'_m = \sum_{m'=-1}^{1} D^{1*}_{mm'}(\alpha, \beta, \gamma) a_{m'}. \tag{B.2}$$

The dipole tensor T, equal to

$$T = 1 - 3\frac{\vec{R}\vec{R}}{R^2}, \tag{B.3}$$

is a traceless tensor of rank 2, the spherical components of which transform according to

$$T'_m = \sum_{m'=-2}^{2} D^{2*}_{mm'}(\phi, \theta, 0) T_{m'} = -\sqrt{6} D^{2*}_{m0}(\phi, \theta, 0), \tag{B.4}$$

because in its own frame T only has the $m = 0$ component nonzero, and $T_0 = -\sqrt{6}$.

Using these expressions, the interaction Hamiltonian (Eq. 2) may be written as

$$\hat{V} = -\frac{\sqrt{6}}{4\pi\epsilon R^3} \sum_{m=-2}^{2} \sum_{m',m''=-1}^{1} (-1)^m C(112; m', -m - m') \times D^{2*}_{m0}(\phi, \theta, 0) D^{1*}_{-m-m',m''}(\alpha, \beta, \gamma)(\hat{\mu}^1)_{m'}(\hat{\mu}^2)_{m''}, \tag{B.5}$$

where the $C(112; m', -m - m')$ are Clebsch-Gordan coefficients. These and the relevant Wigner rotation matrices can all be found in Rose (1957).

As an example we calculate the matrix element for the Q_y-Q_y coupling of the second section. This matrix element is given by

$$V_{0y,0y} = \langle 00|\hat{V}|yy\rangle, \tag{B.6}$$

which contains the transition moments

$$\vec{\mu}_{0y} = \langle 0|\hat{\vec{\mu}}|y\rangle = \mu_y \vec{e}_y, \tag{B.7}$$

where μ_y denotes the magnitude of the transition moment and $\vec{e}_y$ a unit vector in the y direction. In terms of the spherical components this is equal to

$$(\hat{\mu}_{0y})_m = \frac{i}{\sqrt{2}} \mu_y (\delta_{m,1} + \delta_{m,-1}). \tag{B.8}$$

Because these are defined in the molecular frames of the monomers, the expressions are the same for monomer 1 and monomer 2. After some straightforward and rather tedious algebra, we find

$$V_{00,yy} = \frac{\mu_y^2}{4\pi\epsilon R^3}\left(\frac{3}{2}\sin^2\theta[\cos 2\phi(\cos\alpha\cos\gamma - \sin\alpha\sin\gamma\cos\beta) + \sin 2\phi(\sin\alpha\cos\gamma + \cos\alpha\sin\gamma\cos\beta)] - 6\sin\theta\cos\theta\sin\phi\sin\beta\sin\gamma + \left(\frac{3}{2}\cos^2\theta - \frac{1}{2}\right)(\cos\alpha\cos\gamma - \sin\alpha\sin\gamma\cos\beta)\right). \tag{B.9}$$

We also need the inner product for the absorption spectrum, which in terms of the rotation matrices can be written as

$$\hat{\vec{\mu}}^1 \cdot \hat{\vec{\mu}}^2 = \sum_{m=-1}^{1} (-1)^m \sum_{m'=-1}^{1} D^{1*}_{-mm'}(\alpha, \beta, \gamma)(\hat{\mu}^1)_m(\hat{\mu}^2)_{m'}. \tag{B.10}$$

Again, using as an example the $0 \rightarrow y$ transitions, we get

$$(\vec{\mu}^1)_{0y} \cdot (\vec{\mu}^2)_{0y} = \mu_y^2[\cos\alpha\ \gamma - \sin\alpha\sin\gamma\cos\beta]. \tag{B.11}$$

Finally, for the rotational strength we need the combination $\vec{R} \cdot (\hat{\vec{\mu}}^1 \times \hat{\vec{\mu}}^2)$. In terms of the rotation matrices this can be written as

$$\vec{R} \cdot (\hat{\vec{\mu}}^1 \times \hat{\vec{\mu}}^2) = -iR\sqrt{2} \sum_{m,m',m''=-1}^{1} (-1)^m C(111; m', -m - m') \times D^{1*}_{m0}(\phi, \theta, 0) D^{1*}_{-m-m',m''}(\alpha, \beta, \gamma)(\hat{\mu}^1)_{m'}(\hat{\mu}^2)_{m''}. \tag{B.12}$$

For the $0 \rightarrow y$ transitions this becomes

$$\vec{R} \cdot ((\vec{\mu}^1)_{0y} \times (\vec{\mu}^2)_{0y}) = R\mu_y^2[\sin\theta\cos\phi\sin\beta\sin\gamma + \cos\theta(\sin\alpha\cos\gamma + \cos\alpha\cos\beta\sin\gamma)]. \tag{B.13}$$

Expressions B.9, B.11, and B.13 can easily be checked for correctness in various limiting cases.

APPENDIX C: COUPLED TWO-LEVEL SYSTEMS

In this appendix we briefly review the diagonalization procedure for two coupled two-level systems. We use the general notation of Appendix A. The Hamiltonian of the system can be written in matrix form as

$$\mathcal{H} = \begin{pmatrix} E_0^1 + E_0^2 & 0 & 0 & V \\ 0 & E_0^1 + E_1^2 & V & 0 \\ 0 & V & E_1^1 + E_0^2 & 0 \\ V & 0 & 0 & E_1^1 + E_1^2 \end{pmatrix} \tag{C.1}$$

where

$$V = V_{01,10} = V_{10,01} = V_{00,11} = V_{11,00}. \tag{C.2}$$

We note that the matrix can be taken to consist of two blocks, one connecting the ground and double excited states, the other connecting the singly excited states. Both blocks can be diagonalized separately, resulting in the following energies for the eigenstates:

$$E_0 = \frac{1}{2}[E_0^1 + E_1^1 + E_0^2 + E_1^2 - \sqrt{(E_0^1 - E_1^1 + E_0^2 - E_1^2)^2 + 4V^2}]$$

$$E_1 = \frac{1}{2}[E_0^1 + E_1^1 + E_0^2 + E_1^2 - \sqrt{(-E_0^1 + E_1^1 + E_0^2 - E_1^2)^2 + 4V^2}]$$

$$E_2 = \frac{1}{2}[E_0^1 + E_1^1 + E_0^2 + E_1^2 + \sqrt{(-E_0^1 + E_1^1 + E_0^2 - E_1^2)^2 + 4V^2}]$$

$$E_3 = \frac{1}{2}[E_0^1 + E_1^1 + E_0^2 + E_1^2 + \sqrt{(E_0^1 - E_1^1 + E_0^2 - E_1^2)^2 + 4V^2}]. \tag{C.3}$$

The new states can be obtained from the old states by a simple rotation: over an angle ψ_1 for the ground and double excited state, and over an angle ψ_2 for the singly excited states. We can thus write:

$$|0\rangle = \cos\psi_1|00\rangle + \sin\psi_1|11\rangle$$
$$|3\rangle = -\sin\psi_1|00\rangle + \cos\psi_1|11\rangle, \quad \text{(C.4)}$$

where

$$\tan\psi_1 = \frac{E_0 - (E_0^1 + E_0^2)}{V} \quad \text{(C.5)}$$

for the new ground and highest energy states, and

$$|1\rangle = \cos\psi_2|10\rangle + \sin\psi_2|01\rangle$$
$$|2\rangle = -\sin\psi_2|10\rangle + \cos\psi_2|01\rangle, \quad \text{(C.6)}$$

where

$$\tan\psi_2 = \frac{E_1 - (E_1^1 + E_0^2)}{V} \quad \text{(C.7)}$$

for the state corresponding to single excitations.

The various coefficients of Appendix A are thus given by

$$C_{00}^0 = C_{11}^3 = \cos\psi_1 \text{ and } C_{11}^0 = -C_{00}^3 = \sin\psi_1 \quad \text{(C.8)}$$

and

$$C_{10}^1 = C_{01}^2 = \cos\psi_2 \text{ and } C_{01}^1 = -C_{10}^2 = \sin\psi_2. \quad \text{(C.9)}$$

All other coefficients are zero.

The authors thank Henny van Roon for isolating the $\alpha\beta$ subunit, B820, from the LH1 antenna system of *Rs. rubrum* and Raoul Frese (manuscript in preparation) for providing the absorption and CD spectra of B820 (cf. Fig. 1).

REFERENCES

Bradforth, S. E., R. Jimenez, F. van Mourik, R. van Grondelle, and G. R. Fleming. 1995. Excitation transfer in the core light-harvesting complex (LH-1) of *Rhodobacter sphaeroides*: an ultrafast fluorescence depolarization and annihilation study. *J. Phys. Chem.* 99:16179–16191.

Broude, V. L., E. I. Rashba, and E. F. Sheka, editors. 1985. Spectroscopy of Molecular Excitons. Springer-Verlag, New York.

Cantor, C. R., and P. Schimmel. 1980. Biophysical Chemistry. W. H. Freeman and Company, New York.

Chang, M. C., P. M. Callahan, P. S. Parkes-Loach, T. M. Cotton, and P. A. Loach. 1990. Spectroscopic characterization of the light-harvesting complex of *Rhodospirillum rubrum* and its structural subunit. *Biochemistry.* 29:421–429.

Cogdell, R. J., and H. Scheer. 1985. Circular dichroism of light-harvesting complexes from purple photosynthetic bacteria. *Photochem. Photobiol.* 42:669–678.

Craig, D. P., and T. Thirunamachandran. 1984. Molecular Quantum Electrodynamics. Academic Press, San Diego.

De Caro, C., R. W. Visschers, R. van Grondelle, and S. Völker. 1994. Spectral hole burning in pigment-protein complexes of photosynthetic bacteria. *J. Lumin.* 58:149–153.

Fowler, G. J. S., G. D. Sockalingum, B. Robert, and C. N. Hunter. 1994. Blue shifts in bacteriochlorophyll absorbance correlate with changed hydrogen bonding patters in light-harvesting 2 mutants of *Rhodobacter spearoides* with alterations at α-tyr-44 and α-tyr-45. *Biophys. J.* 299: 695–700.

Fowler, G. J. S., R. W. Visschers, G. G. Grief, R. van Grondelle, and C. N. Hunter. 1992. Genetically modified photosynthetic antenna complexes with blueshifted absorbance bands. *Nature.* 355:848–850.

Jimenez, R., S. N. Dikshit, S. E. Bradforth, and G. R. Fleming. 1996. Electronic excitation transfer in the LH2 complex of *Rhodobacter sphaeroides. J. Phys. Chem.* 100:6825–6834.

Karrasch, S., P. Bullough, and R. Ghosh. 1995. The 8.5 Å projection map of the light-harvesting complex I from *Rhodospirillum rubrum* reveals a ring composed of 16 subunits. *EMBO J.* 14:631–638.

Koolhaas, M. H. C., F. van Mourik, G. van der Zwan, and R. van Grondelle. 1994. The B820 subunit of the bacterial light-harvesting antenna, a disordered dimer? *J. Lumin.* 60, 61:515–519.

Kramer, H. J. M., J. D. Pennoyer, R. van Grondelle, W. H. J. Westerhuis, R. A. Niederman, and J. Amesz. 1984a. Low-temperature optical properties and the pigment organization of the B875 light-harvesting bacteriochlorophyll-protein complex of purple photosynthetic bacteria. *Biochim. Biophys. Acta.* 767:335–344.

Kramer, H. J. M., R. van Grondelle, C. N. Hunter, W. H. J. Westerhuis, and J. Amesz. 1984b. Pigment organization of the B800–B850 antenna complex of *Rhodopseudomonas sphaeroides. Biochim. Biophys. Acta.* 765:156–165.

Kühlbrandt, W. 1995. Many wheels make light work. *Nature.* 374: 497–498.

McDermott, G., S. M. Prince, A. A. Freer, A. M. Hawthornthwaite-Lawless, M. Z. Papiz, R. J. Cogdell, and N. W. Isaacs. 1995. Crystal structure of an integral membrane light-harvesting complex from photosynthetic bacteria. *Nature.* 374:517–521.

Parkes-Loach, P. S., J. R. Sprinkle, and P. A. Loach. 1988. Reconstitution of the B873 light-harvesting complex of *Rhodospirillum rubrum* from the separately isolated α- and β-polypeptides and bacteriochlorophyll a. *Biochemistry.* 27:2718–2727.

Pearlstein, R. M. 1991. Chlorophylls. CRC Press, Boca Raton, FL.

Press, W. H., S. A. Teukolsky, B. P. Flannery, and W. T. Vetterling. 1992. Numerical Recipes. Cambridge University Press, New York.

Pullerits, T., R. Monshouwer, F. van Mourik, and R. van Grondelle. 1995. Temperature dependence of electron-vibronic spectra of photosynthetic systems, computer simulations and comparison with experiment. *Chem. Phys.* 194:395–407.

Rose, M. E. 1957. Elementary Theory of Angular Momentum. John Wiley and Sons, New York.

Sauer, K., R. J. Cogdell, S. M. Prince, A. A. Freer, N. W. Isaacs, and H. Scheer. 1996. Structure-based calculations of the optical spectra of LH2 bacteriochlorophyll-protein complex from *Rhodopseudomonas acidophila. Photochem. Photobiol.* 64:564–576.

Scherz, A., and W. W. Parson. 1984. Exciton interactions in dimers of bacteriochlorophyll and related molecules. *Biochim. Biophys. Acta.* 766: 666–678.

Scherz, A., and W. W. Parson. 1986. Interactions of the bacteriochlorophyll in antenna bacteriochlorophyll-protein complexes of photosynthetic bacteria. *Photosynth. Res.* 9:21–32.

Scherz, A., V. Rosenbach-Belkin, and J. R. E. Fisher. 1990. Distribution and self-organization of photosynthetic pigments in micelles: implication for the assembly of light-harvesting complexes and reaction centers in the photosynthetic membrane. *Proc. Natl. Acad. Sci. USA.* 87: 5430–5434.

Somsen, O. J. G. 1995. Excitonic Interaction in Photosynthesis. PhD thesis, Vrije Universiteit Amsterdam.

Somsen, O. J. G., R. van Grondelle, and H. van Amerongen. 1996. Spectral broadening of interacting pigments, polarized absorption by photosynthetic proteins. *Biophys J.* 71:1934–1951.

Van Mourik, F., C. J. R. van der Oord, K. J. Visscher, P. S. Parkes-Loach, P. A. Loach, R. W. Visschers, and R. van Grondelle. 1991. Exciton interactions in the light-harvesting antenna of photosynthetic bacteria studied with triplet-singlet spectroscopy and singlet-triplet annihilation on the B820 subunit form of *Rhodospirillum rubrum. Biochim. Biophys. Acta.* 1059:111–119.

Van Mourik, F., R. W. Visschers, M. C. Chang, R. J. Cogdell, V. Sundström, and R. van Grondelle. 1990. Membrane-Bound Complexes in Phototropic Bacteria. Plenum Press, New York.

Van Mourik, F., R. W. Visschers, and R. van Grondelle. 1992. Energy transfer and aggregate size effects in the inhomogeneously broadened core light-harvesting complex of *Rhodobacter sphaeroides*. *Chem. Phys. Lett.* 195:1–7.

Visschers, R. W., M. C. Chang, F. van Mourik, P. S. Parkes-Loach, B. A. Heller, P. A. Loach, and R. van Grondelle. 1991. Fluorescence polarization and low-temperature absorption spectroscopy of a subunit form of light-harvesting complex I from purple photosynthetic bacteria. *Biochemistry.* 30:5734–5742.

Visschers, R. W., R. Nunn, F. Calkoen, F. van Mourik, C. N. Hunter, D. W. Rice, and R. van Grondelle. 1992. Spectroscopic characterization of B820 subunits from light-harvesting complex I of *Rhodospirillum rubrum* and *Rhodobacter sphaeroides* prepared with the detergent *n*-octyl-*rac*-2,3-dipropylsulfoxide. *Biochim. Biophys. Acta.* 1100:259–266.

Visschers, R. W., F. van Mourik, R. Monshouwer, and R. van Grondelle. 1993. Inhomogeneous spectral broadening of B820 subunit forms of LH1. *Biochim. Biophys. Acta.* 1141:238–244.

Visser, H. M., O. J. G. Somsen, F. van Mourik, S. Lin, I. H. M. van Stokkum, and R. van Grondelle. 1995. Direct observation of subpicosecond equilibration of excitation energy in the light-harvesting antenna of the *Rhodospirillum rubrum*. *Biophys. J.* 69:1083–1099.